

Magneto-optical properties of $\text{La}_{0.7}\text{Sr}_{0.3}\text{MnO}_3$ thin films with perpendicular magnetic anisotropy

H. L. Liu,^{a)} K. S. Lu, and M. X. Kuo

Department of Physics, National Taiwan Normal University, Taipei 116, Taiwan

L. Uba and S. Uba

Institute of Experimental Physics, University of Bialystok, Lipowa 41, PL-15-424 Bialystok, Poland

L. M. Wang

Department of Electrical Engineering, Da-Yeh University, Changhua 112, Taiwan

H.-T. Jeng

Physics Division, National Center for Theoretical Sciences, Hsinchu 300, Taiwan

(Received 1 August 2005; accepted 10 January 2006; published online 28 February 2006)

We report the magneto-optical (MO) properties of compressively strained $\text{La}_{0.7}\text{Sr}_{0.3}\text{MnO}_3$ (LSMO) thin films epitaxially grown on a LaAlO_3 substrate. The magnetic force microscope images show the stripe magnetic domains, characteristic of films with the perpendicular magnetic anisotropy (PMA). The optical reflectance and transmittance of the samples were measured over a broad energy range from the far infrared through the ultraviolet. To extract the optical constants of the films, we analyzed all of the layers of this thin-film structure using a Drude-Lorentz model. From the parameters obtained, we compute the optical constants, such as frequency-dependent optical conductivity and the diagonal components of the dielectric tensor. Moreover, the MO polar Kerr spectra of the samples were measured in an applied magnetic field of 1.5 T between 0.74 and 5.8 eV. The off-diagonal components of the dielectric tensor were then calculated by analyzing Kerr rotation, ellipticity, and the determined diagonal elements of the dielectric tensor. These functions yield information about the spin-dependent electronic structures of the LSMO thin films. We observed several MO-active transitions above 2 eV. These bands arise from the $\text{Mn-}d(t_{2g})$ to $\text{Mn-}d(e_g)$ in the majority-spin channel and the onset of $\text{O-}2p$ to $\text{Mn-}d(e_g)$ and $\text{O-}2p$ to $\text{Mn-}d(t_{2g})$ transitions in the minority-spin channel, in accord with the band-structure calculations. Most interestingly, their peak position and intensity are dependent on the film thickness, suggesting possible applications for tailoring MO responses in these PMA thin films. © 2006 American Institute of Physics. [DOI: 10.1063/1.2173681]

I. INTRODUCTION

The hole doped manganite perovskites $R_{1-x}A_x\text{MnO}_3$ (Refs. 1 and 2) (R and A being trivalent rare-earth and divalent alkaline-earth ions, respectively) have recently attracted enormous attention, stimulated not only the potential technological usefulness of their colossal magnetoresistance (CMR) effect^{3,4} but also for the need to understand the mechanism underlying their unusual magnetic and transport properties.^{5,6} Among a number of perovskite-type manganese oxides with various combinations of (R, A), $\text{La}_{1-x}\text{Sr}_x\text{MnO}_3$ is considered to be a prototypical and reference material. The parent compound LaMnO_3 is an antiferromagnetic insulator with the Néel temperature $T_N \sim 140$ K. The ferromagnetic state of $\text{La}_{1-x}\text{Sr}_x\text{MnO}_3$ appears below the Curie temperature T_C and above a critical composition of $x_c \sim 0.17$ and develops up to $T_C \sim 380$ K at the doping level of $x = 0.3-0.5$.⁷

There has been particular interest recently in the $\text{La}_{0.7}\text{Sr}_{0.3}\text{MnO}_3$ (LSMO) thin film due to its half-metallic nature, i.e., the majority-spin electrons show a metallic behavior, while the minority-spin electrons have an electronic structure of a semiconductor. Consequently, the conduction

electrons are found to be 100% spin polarized at the Fermi level.⁸ This exotic physical property has a significant effect on technological applications related to magnetism and spin electronics. Knowledge of the spin-dependent electronic structures of LSMO is therefore desirable for the use of these films as magnetic devices. Optical reflectance/transmittance measurements have been used to investigate the electronic structure of manganites;⁹ however, the experimental data and their interpretations are varied. Furthermore, the optical spectra do not show a pronounced fine structure; as a consequence the information obtained from the optical spectra about the electronic structure is not very detailed but is mainly limited to the joint density of states. In contrast, the magneto-optical (MO) Kerr effect is a different technique. The Kerr spectra provide not only the information about the joint density of states but also the electron spin polarization of states participating in the MO transitions.

Few studies of the MO properties of LSMO have been reported in the past. The MO spectral measurements of the LSMO polycrystalline thin-film samples¹⁰ and epitaxial films on SrTiO_3 substrate^{11,12} show the similar characteristic behavior, in which the Kerr rotation reaches the maximum near 3.2 eV. However, these MO results differ strongly from

^{a)}Electronic mail: hliu@phy.ntnu.edu.tw

those of the corresponding bulk polycrystalline pellets and single crystals.^{13,14} It has been demonstrated that the films have different physical properties compared to bulk materials due to lattice and thermal mismatch between the film and the substrate.^{15–21} In this paper, we focus on thin films of LSMO on a LAO substrate. The biaxial compressive strain of LSMO on LAO is predicted to give rise to the perpendicular magnetic anisotropy (PMA) behavior.^{15,17,20} We carefully study the optical and MO properties of these LSMO thin films with different thicknesses. This work is different from earlier MO studies,^{10–14} as we use the reflectance and transmittance to extract directly the optical constants such as frequency-dependent optical conductivity and the diagonal components of the dielectric tensor. The off-diagonal components of the dielectric tensor were then calculated by analyzing Kerr rotation, ellipticity, and the determined diagonal elements of the dielectric tensor. Our overall goal is to obtain the full dielectric tensor for the LSMO thin films, which has connotations for the physics of the half-metallic ferromagnetism as well as potential utility for understanding the MO Kerr effect in LSMO-based devices that may exploit the properties of these materials.

II. EXPERIMENT

LSMO thin films with thicknesses ranging from 50 to 300 nm were deposited on the LaAlO₃ (001) substrate by the off-axis magnetron sputtering technique described previously.²² The x-ray powder-diffraction results show that each of our films is of purely single phase. Generally, bulk LSMO has a pseudocubic lattice parameter of 0.387 nm, whereas the LaAlO₃ has a cubic lattice parameter of 0.379 nm. The lattice mismatch between them is thus 2.07% and this leads to a considerable strain in the *a-b* plane of the epitaxial films. Indeed, the observed *c*-axis lattice parameter increases from a value of 0.388 nm for the 300-nm-thick film up to 0.394 nm for the 50-nm-thick film. The magnetic properties determined with a superconducting quantum-interference device magnetometer also show that the films have different *T_C* compared to bulk material due to the strain effect. The value of *T_C* for the 50-nm-thick film is 40 K lower than the bulk value. It should be emphasized that the observed changes in *T_C* of the films are not due to the effects of different oxygen stoichiometry,^{23–25} since we grow all the films of varying thicknesses while maintaining identical conditions.

The room-temperature reflectance \mathfrak{R} and transmittance \mathfrak{T} measurements were performed over a wide frequency region between 50 and 55 000 cm⁻¹. A Bruker IFS 66v Fourier transform infrared spectrometer was used in the far-infrared and mid-infrared regions (50–6000 cm⁻¹), while the near-infrared to near-ultraviolet regions (4000–55 000 cm⁻¹) were covered using a Perkin-Elmer Lambda-900 spectrometer. The films with $d \leq 100$ nm were studied in both \mathfrak{R} and \mathfrak{T} . To deal with the dispersion and absorption in the substrate, the reflectance $\mathfrak{R}_{\text{sub}}$ and transmittance $\mathfrak{T}_{\text{sub}}$ were also measured. The absorption coefficient $\alpha(\omega)$ and the index refraction $n(\omega)$ of the substrate and the multilayer Drude-Lorentz

model were then used in the analysis of the data for films. The 300-nm-thick film was studied only in \mathfrak{R} .

We have used thin-film optics and the Drude-Lorentz analysis to model the optical properties of these samples. The thin-film optics problem²⁶ begins with a single layer of thickness d_1 and the complex index of refraction \tilde{n}_1 located between two semi-infinite media with indices of refraction \tilde{n}_0 and \tilde{n}_2 . Although the light experiences multiple reflections within the thin layer, one may use the resultant electric-field vectors and match boundary conditions at the two interfaces. This approach yields a matrix equation:

$$\begin{pmatrix} 1 \\ \tilde{n}_0 \end{pmatrix} + \begin{pmatrix} 1 \\ -\tilde{n}_0 \end{pmatrix} r_1 = M_1 \begin{pmatrix} 1 \\ \tilde{n}_2 \end{pmatrix} t_1, \quad (1)$$

where we have assumed the unit amplitude for the incident electric-field vector. The coefficient r_1 is then the amplitude of the reflected resultant electric-field vector at the first interface, and t_1 is the amplitude of the resultant transmitted field behind the interface. The quantity M_1 is known as the transfer matrix of the single layer; it is given by

$$M_1 = \begin{pmatrix} \cos \delta_1 & \frac{-i}{\tilde{n}_1} \sin \delta_1 \\ -i\tilde{n}_1 \sin \delta_1 & \cos \delta_1 \end{pmatrix}. \quad (2)$$

This matrix contains all the information about a single layer: the complex index of refraction and the thickness of the layer are contained in $\delta_1 = (2\pi/\lambda)\tilde{n}_1 d_1 \cos \theta$. If one solves the matrix equation for r_1 and t_1 , the reflectance and transmittance of the layer can be written as

$$\mathfrak{R}_1 = r_1 r_1^*, \quad \mathfrak{T}_1 = \frac{\tilde{n}_2}{\tilde{n}_0} t_1 t_1^*. \quad (3)$$

Knowing \tilde{n}_1 and thickness d , we can calculate the reflectance and transmittance of the film.

This approach extends in a straightforward way to an N -layer system.²⁶ Each transfer matrix carries information for one layer, and the resultant transfer matrix M_N is simply the product of all transfer matrices for the N layer, i.e., $M_N = M_1 M_2 \dots M_n$, where M_n is the transfer matrix of the n th layer. Regarding M_1 with M_N in Eq. (1) allows the calculation of the reflectance and transmittance of the N -layer system, assuming that one knows all the $\tilde{n}_i = \sqrt{\tilde{\epsilon}_i}$, where $\tilde{\epsilon}_i$ is the complex dielectric function of layer i .

The Drude-Lorentz model²⁷ used for the complex dielectric function of each layer may be written as

$$\tilde{\epsilon}(\omega) = -\frac{\omega_{pD}^2}{\omega^2 + i\omega/\tau_D} + \sum_{j=1}^N \frac{\omega_{pj}^2}{\omega_j^2 - \omega^2 - i\omega\gamma_j} + \epsilon_\infty, \quad (4)$$

where ω_{pD} and $1/\tau_D$ are the plasma frequency and the scattering rate of the Drude component; ω_j , γ_j , and ω_{pj} are the frequency, damping, and oscillator strength of the j th Lorentzian contribution; and ϵ_∞ is the high frequency limit of $\tilde{\epsilon}(\omega)$ which includes interband transitions at frequencies above the measured range. Our procedure consists of fitting the measured reflectance and transmittance using the Drude-Lorentz model for each of the two layers in our samples, adjusting

the parameters (including the layer thickness) for a best fit to both measured quantities.

The polar Kerr rotation θ_k and ellipticity η_k spectra were measured at room temperature with a MO spectrometer based on the polarization modulation technique²⁸ over the photon energy range of 0.74–5.8 eV. The angle of incidence of the light on the sample surface mounted inside the 1.5 T water-cooled electromagnet was 3°. The setup was also used to measure θ_k and η_k hysteresis loops at fixed light wavelength. The sensitivity of the MO spectrometer is the order 10^{-4} – 10^{-5} deg. In the polar geometry, where the z axis is chosen to be perpendicular to the solid surface and parallel to the magnetization direction, the expression for the complex Kerr angle is given by²⁹

$$\theta_k(\omega) + i\eta_k(\omega) = \frac{i\tilde{\epsilon}_{xy}(\omega)}{\sqrt{\tilde{\epsilon}_{xx}(\omega)[\tilde{\epsilon}_{xx}(\omega) - 1]}}, \quad (5)$$

where $\tilde{\epsilon}_{xx}$ and $\tilde{\epsilon}_{xy}$ are the diagonal and off-diagonal parts of the complex dielectric tensor, respectively.

III. RESULTS AND DISCUSSION

The room-temperature reflectance and transmittance spectra of the LAO substrate and the three films with different thicknesses are shown in Fig. 1, along with the fitting results. The parameters used to fit the measured optical data are listed in Table I. For the 50- and 100-nm-thick films, there is a small transmitted intensity ($\mathcal{T} < 20\%$) in the far-infrared region below 100 cm^{-1} , and \mathcal{T} reaches 20% above 1000 cm^{-1} . The LAO substrate prevents any transmittance over 100 – 800 cm^{-1} due to phonon processes. While four infrared-active phonon bands between 100 and 800 cm^{-1} are observed in the reflectance spectra. For higher frequencies, the spectra are almost dispersionless, showing only several weak electronic features. In the case of the 300-nm-thick film, it is opaque in the entire frequency region. Notably, the reflectance values we measured in the region below 10000 cm^{-1} are lower than those taken in LSMO single crystal,³⁰ suggesting a lower conductivity in our film likely due to grain boundaries and internal strain.

Figure 2 shows the frequency-dependent optical conductivity $\sigma_1(\omega)$ of the LAO substrate and the three films. There are three notable features seen in the conductivity spectrum of the 50-nm-thick film: first, the four infrared-active phonon bands near 180 , 348 , 424 , and 610 cm^{-1} have frequencies consistent with the external mode of the rare-earth ions and the bending or stretching modes of the MnO_6 octahedra, respectively;^{31,32} second, no Drude peak at zero frequency and a broad absorption band in the mid-infrared region,^{33–36} and third, an optical excitation near 36000 cm^{-1} that can be associated with charge-transfer transition between O $2p$ and Mn $3d$ states.^{33–36} It is worth mentioning that the strongly thickness-dependent evolution of the mid-infrared band likely reflects the changes of the polaron formation energy, caused by the strain-induced electron-phonon coupling.^{37,38} Moreover, the charge-transfer band shows a shift of the peak position to higher frequencies for decreasing thickness of films mainly due to the contraction effects of the a - b plane.³⁸

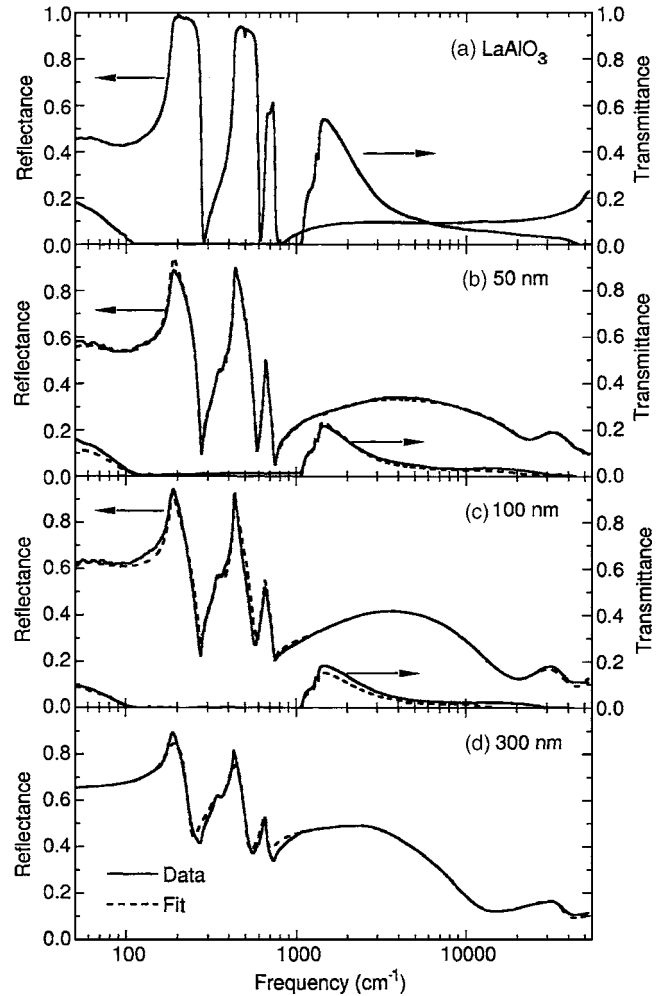


FIG. 1. Room-temperature measured reflectance and transmittance of the LAO substrate and the three LSMO films (solid lines). The dashed lines are the best fit using the thin-film optics and the Drude-Lorentz model.

In Fig. 3 we show the diagonal elements of the dielectric tensor of three films. These spectra were obtained from the analysis of the multilayer Drude-Lorentz model and were subsequently used in the calculation of the off-diagonal elements of the dielectric tensor from the Kerr measurements. We first notice that the positive value of $\text{Re}[\tilde{\epsilon}_{xx}]$ at low frequencies in all three films is an indication of no free-carrier contributions.³⁹ Second, the spectrum of the 50-nm-thick film is quite similar to that of the $\text{La}_{0.7}\text{Ca}_{0.3}\text{MnO}_3$ film with the same thickness and just below the metal-insulator transition temperature.⁴⁰ Third, no clear trends with various thicknesses are apparent in these spectra. This is due to the fact that $\tilde{\epsilon}_{xx}$ is composed of a large number of overlapping optical transitions, each possibly having a different dependence on, as well as energy shift with, the variation of the film thickness.

The ferromagnetic ordering temperature of our LSMO thin films is in the range of 327 – 352 K . Figure 4 presents the magnetic-field dependence of η_k , measured in the polar Kerr geometry at a photon energy of 1.26 eV and with out-of-plane orientation of the applied magnetic field. For the 300-nm-thick film, η_k saturates at nearly 0.053° in an external field of 5 kOe , but the η_k magnitude is strongly reduced

TABLE I. Parameters of a Drude-Lorentz fit for the measured optical data. All units are in cm^{-1} .

Thickness	50 nm	100 nm	300 nm
ω_{p1}	947	825	1 146
ω_1	180	180	180
γ_1	64	40	28
ω_{p2}	492	480	505
ω_2	348	348	348
γ_2	41	42	40
ω_{p3}	1 247	1 442	1 498
ω_3	424	424	420
γ_3	35	64	58
ω_{p4}	1 205	722	748
ω_4	610	619	650
γ_4	105	117	47
ω_{p5}	18 112	19 077	9 789
ω_5	3 630	3 220	2 852
γ_5	17 410	16 972	3 067
ω_{p6}	30 680	33 547	22 165
ω_6	7 737	8 628	6 005
γ_6	45 500	35 443	11 775
ω_{p7}	47 746	30 500	31 809
ω_7	36 050	35 567	34 890
γ_7	23 350	17 813	13 534
ϵ_∞	4.5	4.5	4.5

with the decrease of film thickness. It can also be seen that the polar Kerr loops of all three films show a linear-field dependence, characteristic for the system of PMA, where the alternatively up and down stripe magnetic domains exist.^{41–44} Indeed, the magnetic force microscope (MFM) image of the 300-nm-thick film, shown in the inset of Fig. 4, displays labyrinthine stripe magnetic domains with an average width of 100 nm,⁴⁵ from which the out-of-plane magnetization component confirms the persisted PMA.⁴⁶ The polar Kerr rotation θ_k and ellipticity η_k spectra of three films measured under saturation conditions are shown in Figs. 5(a) and 5(b), respectively. The Kramers-Kronig relation seems to be fulfilled between θ_k and η_k , which were independently deduced. It was found that the maximum values of θ_k and η_k at room temperature for the 300-nm-thick film are 0.32° at about 3.4 eV and 0.24° at about 3.9 eV, respectively. In addition, the characteristic behavior in our spectra is qualitatively similar to three earlier studies^{10–12} but appears to disagree with those reported on corresponding polycrystalline pellets and single crystals.^{13,14}

As the magnitude of the Kerr spectra depends on the film thickness, the effect of multiple reflection of the light in the film on the substrate, in particular, for the thinnest film samples, can be important. To obtain the intrinsic MO properties of LSMO films itself, we applied the so-called multiple-reflection calculation.^{47,48} The off-diagonal elements of the dielectric tensor of three films calculated with the use of the multiple-reflection analysis are shown in Figs. 6(a) and 6(b). One first observes that the magnitude of the

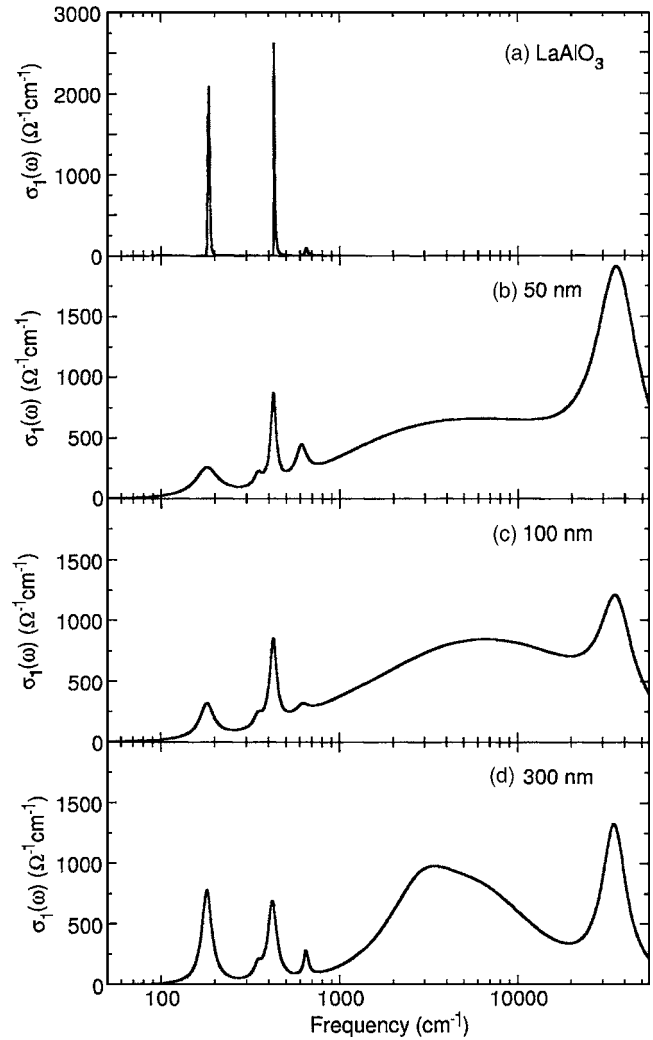


FIG. 2. The room-temperature optical conductivity of the LAO substrate and the three LSMO films computed from the fitting parameters listed in Table I.

off-diagonal components of the dielectric tensor of all three films is smaller than that of the diagonal ones by a factor of 10^2 . Second, the $\text{Re}[\tilde{\epsilon}_{xy}]$ and $\text{Im}[\tilde{\epsilon}_{xy}]$ spectra of three films exhibit a similar overall structure, but some differences are clearly visible in the energy range of 2.5–3.2 eV. The main spectral features are located at the same energies in the range above 3.3 eV. All the films show a strong negative peak at about 3.3 eV and two positive peaks at about 4.1 and 4.7 eV in the $\text{Re}[\tilde{\epsilon}_{xy}]$ spectra. The $\text{Im}[\tilde{\epsilon}_{xy}]$ spectra show a positive two-peak structure at about 2.5 and 3.1 eV in the 300-nm-thick film, a single peak at about 2.5 eV in the 100-nm-thick film, a broad peak centered at about 2.8 eV in the 50-nm-thick film, and the largest negative peak at about 3.6 eV in all three films. The observed differences between the spectra magnitude in three films can be due to different magnetization resulting from the sample thickness related reduction of the ferromagnetic ordering temperature.

In principle, the electronic transitions that appear in the $\tilde{\epsilon}_{xy}(\omega)$ spectra will fall into two classes. In the first case, the contribution to $\tilde{\epsilon}_{xy}(\omega)$ is dominated by the energy splitting between excited states, for instance, a transition between an orbital singlet ground state and a spin-orbit split excited

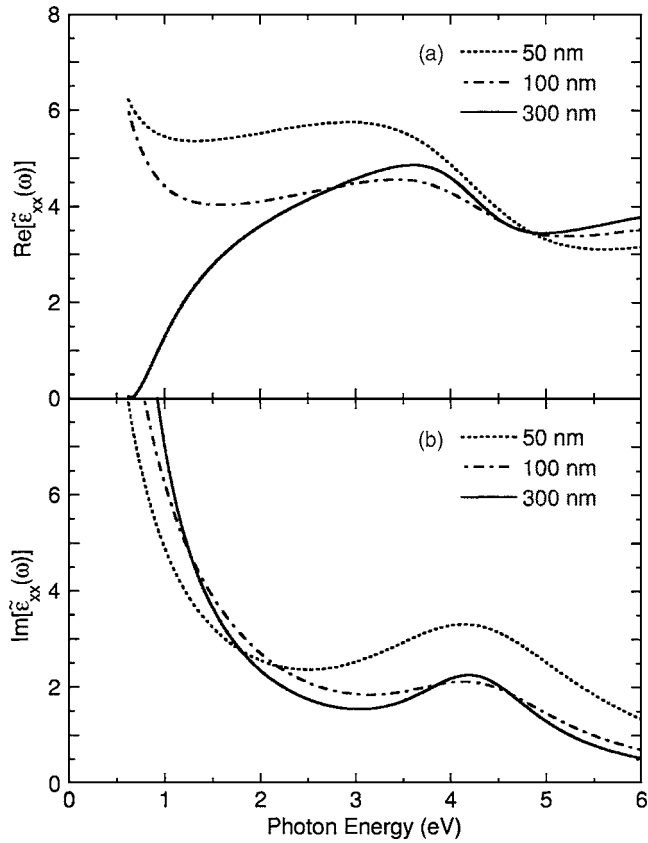


FIG. 3. The real and imaginary parts of the diagonal components of the dielectric tensor of the three LSMO films.

state. A so-called type-I line shape is observed: $\text{Re}[\tilde{\epsilon}_{xy}]$ exhibits a dissipation-type spectrum in which the peak (or dip) appears at the transition frequency ω_0 . The corresponding $\text{Im}[\tilde{\epsilon}_{xy}]$ shows, on the other hand, a dispersion type around ω_0 . This is historically called a diamagnetic line shape. In the

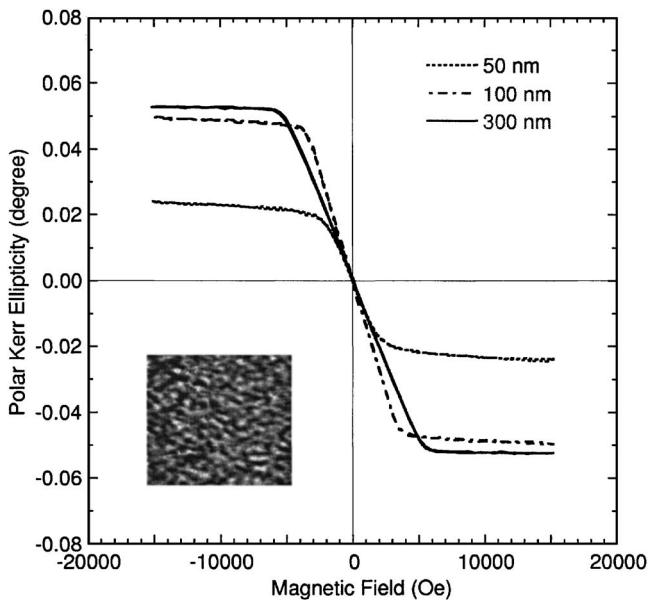


FIG. 4. The magnetic-field dependence of the polar Kerr ellipticity of the three LSMO films measured at a photon energy of 1.26 eV. The inset shows the MFM image of the 300-nm-thick film taken at room temperature. The scan size is $4 \times 4 \mu\text{m}^2$.

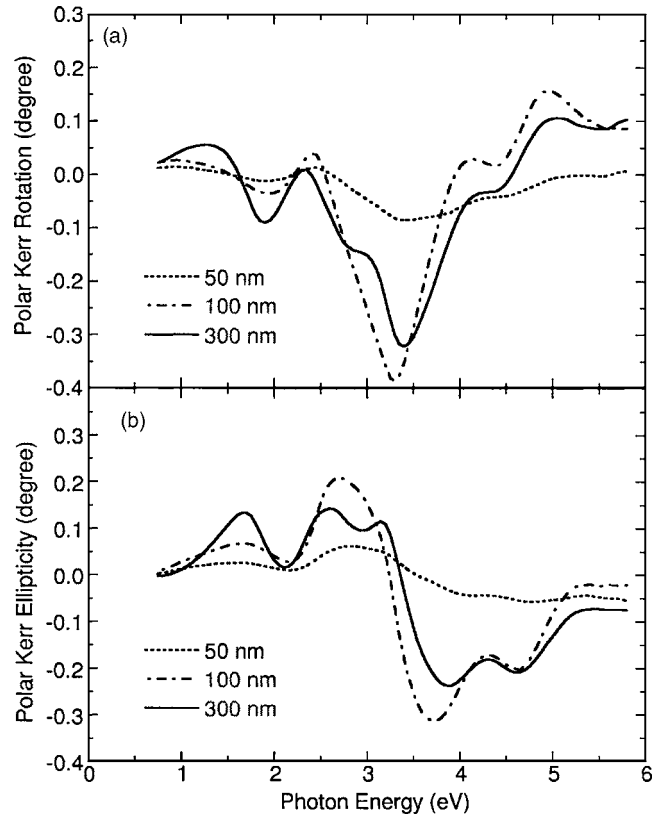


FIG. 5. Experimental polar Kerr rotation and ellipticity spectra of the three LSMO films.

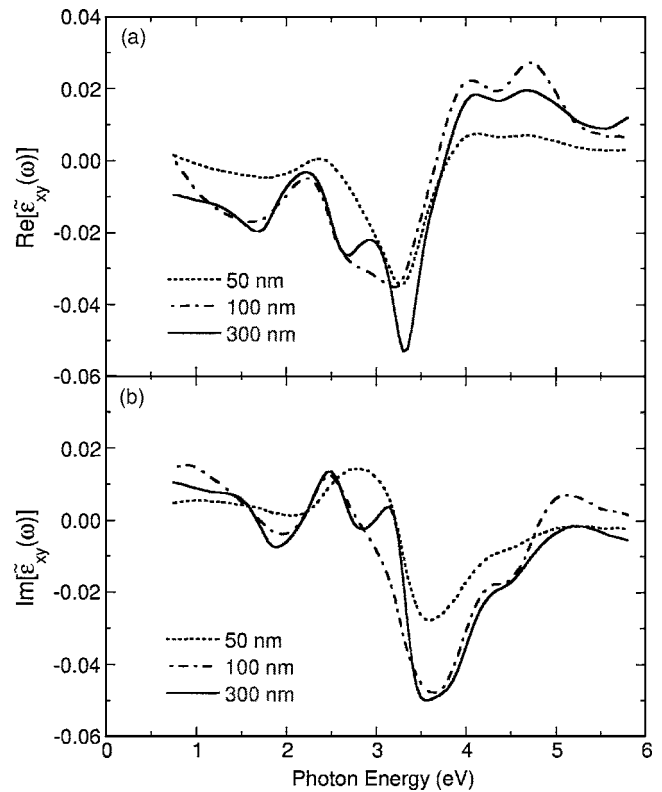


FIG. 6. The calculated real and imaginary parts of the off-diagonal elements of the dielectric tensor of the three LSMO films.

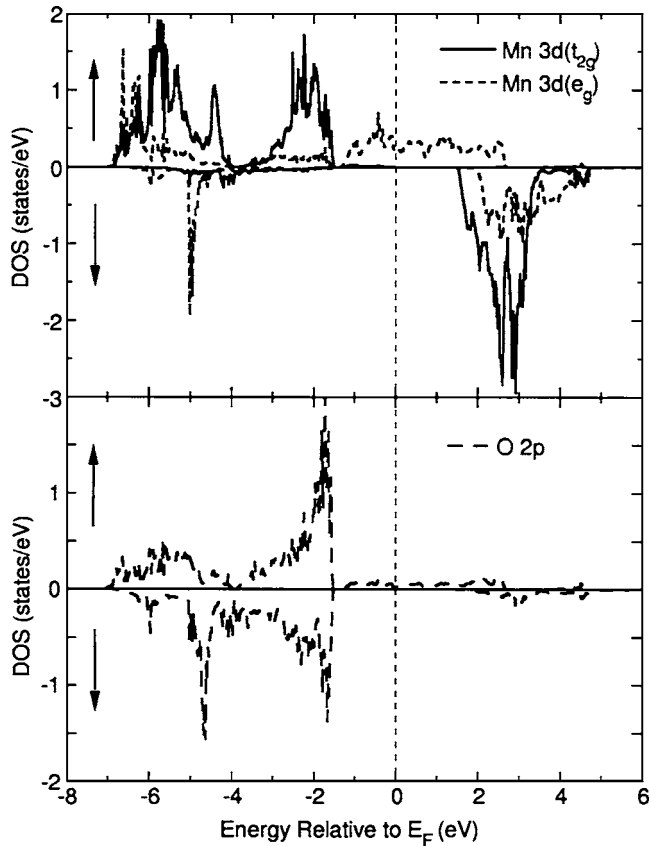


FIG. 7. The Mn 3d and O 2p partial densities of states of LSMO obtained from the LDA+ U calculation. The Mn 3d band is decomposed into t_{2g} (solid lines) and e_g (dashed lines) bands.

second case, the contribution to $\tilde{\epsilon}_{xy}(\omega)$ is dominated by a difference in ground-state population of the levels of a spin-orbit split ground state, for example, a transition between an orbitally degenerate ground state and an orbital singlet excited state. A so-called type-II line shape is observed: $\text{Re}[\tilde{\epsilon}_{xy}]$ shows a dispersion-type shape centered at ω_0 while $\text{Im}[\tilde{\epsilon}_{xy}]$ has a dissipation-type one. This is historically called a paramagnetic line shape. Thus, the observed MO transitions in the 300-nm-thick film at around 3.3, 4.1, and 4.7 eV are sorted into the type I, while the features at around 2.5, 3.1, and 3.6 eV correspond to the type-II transitions.

We now discuss the origin of these MO spectral features. There has been only one theoretical investigation attempted to the MO properties for octahedrally coordinated Mn^{3+} systems.⁴⁹ However, as mentioned above, only transitions from or to states with nonzero orbital moment can contribute to $\tilde{\epsilon}_{xy}(\omega)$. The cubic crystal field quenches the orbital moment in the Mn- $d(e_g)$ states. Therefore, only transitions involving the Mn- $d(t_{2g})$ states contribute significantly as only those states carry a considerable orbital moment. Here, we have performed the electronic structure calculations for LSMO by using full-potential projected augmented wave method⁵⁰ as implemented in the Vienna *ab initio* simulation package⁵¹ (VASP) within the framework of LDA+ U scheme.⁵² The parameters used in this calculation are the Coulomb correlation $U=4.0$ eV and the exchange correlation $J=0.87$ eV for Mn 3d electrons, while $U=5.0$ eV and $J=0.95$ eV for La 4f electrons.⁵³ Figure 7 shows the partial

densities of states (DOSs) for the Mn 3d and O 2p electrons. There are several important features to these results. First, our LDA+ U calculation indicates a half-metallic ground state for LSMO. Second, it is likely that the type-II peaks at about 2.5 and 3.1 eV originate from Mn- $d(t_{2g})$ to Mn- $d(e_g)$ transitions within the majority-spin channel, which is enabled by the p - d hybridization. The absorption band at about 3.6 eV is due to a charge-transfer excitation between O-2p and Mn- $d(e_g)$ states in the minority-spin channel. In addition, only transitions from O-2p to Mn- $d(t_{2g})$ states in the minority-spin channel contribute significantly forming the major part of the type-I peaks at about 3.3, 4.1, and 4.7 eV.

IV. SUMMARY

In summary, we have measured the optical and MO Kerr spectra of the LSMO thin films. Compressive strain induced by growth on a LAO substrate results in a spontaneous out-of-plane magnetization. The off-diagonal components of the dielectric tensor were calculated by analyzing Kerr rotation, ellipticity, and the determined diagonal elements of the dielectric tensor. Several charge-transfer-type MO spectra are observed above 2 eV and their peak position and intensity are found to be sensitive to the film thickness. These are likely to arise from the Mn- $d(t_{2g})$ to Mn- $d(e_g)$ in the majority-spin channel and the onset of O-2p to Mn- $d(e_g)$ and O-2p to Mn- $d(t_{2g})$ transitions in the minority-spin channel, in accord with the band-structure calculations. Our data clearly show that accurate values for diagonal and off-diagonal components of the dielectric tensor are important not only for the spin-polarized band-structure studies but also for a potential application of the PMA in these ferromagnetic LSMO thin films.

ACKNOWLEDGMENTS

We would like to gratefully acknowledge financial support from the National Science Council of Taiwan under Grant Nos. NSC 94-2112-M-003-002 and 94-2120-M-007-013, and the National Taiwan Normal University under Grant No. ORD93-B.

- ¹G. H. Jonker and J. H. Van Santen, *Physica (Amsterdam)* **16**, 337 (1950).
- ²J. E. O. Wollan and W. C. Koehler, *Phys. Rev.* **100**, 545 (1955).
- ³R. M. von Helmolt, J. Wecker, B. Holzappel, L. Schultz, and K. Samwer, *Phys. Rev. Lett.* **71**, 2331 (1993).
- ⁴S. Jin, T. H. Tiefel, M. McCormack, R. A. Fastnacht, R. Ramesh, and L. H. Chen, *Science* **264**, 413 (1994).
- ⁵P. Schiffer, A. P. Ramirez, W. Bao, and S.-W. Cheong, *Phys. Rev. Lett.* **75**, 3336 (1995).
- ⁶A. P. Ramirez, *J. Phys.: Condens. Matter* **9**, 8171 (1997).
- ⁷A. Urushibara, Y. Moritomo, T. Arima, A. Asamitsu, G. Kido, and Y. Tokura, *Phys. Rev. B* **51**, 11103 (1995).
- ⁸J.-H. Park, E. Vescovo, H.-J. Kim, C. Kwon, R. Ramesh, and T. Venkatesan, *Nature (London)* **392**, 794 (1998).
- ⁹T. W. Noh, J. H. Jung, and K. H. Kim, *Physics of Manganites*, edited by T. A. Kaplan and S. D. Mahanti (Plenum, New York, 1999), and references therein.
- ¹⁰J. Cho, M. Gomi, and M. Abe, *Jpn. J. Appl. Phys., Part 1* **29**, 1686 (1990).
- ¹¹P. Fumagalli, C. Spaeth, and G. Güntherodt, *IEEE Trans. Magn.* **31**, 3277 (1995).
- ¹²M. Koubaa *et al.*, *J. Magn. Magn. Mater.* **272–276**, 1812 (2004).
- ¹³T. J. A. Popma and M. G. J. Kammaing, *Solid State Commun.* **17**, 1073 (1975).

- ¹⁴S. Yamaguchi, Y. Okimoto, K. Ishibashi, and Y. Tokura, *Phys. Rev. B* **58**, 6862 (1998).
- ¹⁵C. Kwon *et al.*, *J. Magn. Magn. Mater.* **172**, 229 (1997).
- ¹⁶Y. Suzuki, H. Y. Hwang, S.-W. Cheong, and R. B. van Dover, *Appl. Phys. Lett.* **71**, 140 (1997).
- ¹⁷Y. Wu, Y. Suzuki, U. Rüdiger, J. Yu, A. D. Kent, T. N. Nath, and C. B. Eom, *Appl. Phys. Lett.* **75**, 2295 (1999).
- ¹⁸X. W. Wu, M. S. Rzchowski, H. S. Wang, and Q. Li, *Phys. Rev. B* **61**, 501 (2000).
- ¹⁹F. S. Razavi, G. M. Gross, H.-U. Habermeier, O. Lebedev, S. Amelinckx, G. Van Tendeloo, and A. Vigliante, *Appl. Phys. Lett.* **76**, 155 (2000).
- ²⁰R. Desfeux, S. Bailleul, A. Da Costa, W. Prellier, and A. M. Haghiri-Gosnet, *Appl. Phys. Lett.* **78**, 3681 (2001).
- ²¹Z. H. Wang, H. Kronmüller, O. I. Lebedev, G. M. Gross, F. S. Razavi, H.-U. Habermeier, and B. G. Shen, *Phys. Rev. B* **65**, 054411 (2002).
- ²²L. M. Wang, H. H. Sung, B. T. Su, H. C. Yang, and H. E. Horng, *J. Appl. Phys.* **88**, 4236 (2000).
- ²³G. C. Xiong, Q. Li, H. L. Ju, R. L. Greene, and T. Venkatesan, *Appl. Phys. Lett.* **66**, 1689 (1995).
- ²⁴M. Rajeswari *et al.*, *Appl. Phys. Lett.* **73**, 2672 (1998).
- ²⁵J. Dho, N. H. Hur, I. S. Kim, and Y. K. Park, *J. Appl. Phys.* **94**, 7670 (2003).
- ²⁶O. S. Heavens, *Optical Properties of Thin Solid Films* (Dover, New York, 1965).
- ²⁷F. Wooten, *Optical Properties of Solids* (Academic, New York, 1972).
- ²⁸K. Sato, *Jpn. J. Appl. Phys.* **20**, 2403 (1981).
- ²⁹W. Reim and J. Schoenes, in *Ferromagnetic Materials*, edited by E. P. Wohlfarth and K. H. J. Buschow (North-Holland, Amsterdam, 1990), Vol. 5, p. 133.
- ³⁰Y. Okimoto, T. Katsufuji, T. Ishikawa, T. Arima, and Y. Tokura, *Phys. Rev. B* **55**, 4206 (1997).
- ³¹M. N. Illiev, M. V. Abrashev, H.-G. Lee, V. N. Popov, Y. V. Sun, C. Thomsen, R. L. Mens, and C. W. Chu, *Phys. Rev. B* **57**, 2872 (1998).
- ³²I. Fedorov *et al.*, *Phys. Rev. B* **60**, 11875 (1999).
- ³³Y. Okimoto, T. Katsufuji, T. Ishikawa, A. Urushibara, T. Arima, and Y. Tokura, *Phys. Rev. Lett.* **75**, 109 (1995).
- ³⁴S. G. Kaplan, M. Quijada, H. D. Drew, D. B. Tanner, G. C. Xiong, R. Ramesh, C. Kwon, and T. Venkatesan, *Phys. Rev. Lett.* **77**, 2081 (1996).
- ³⁵J. H. Jung, K. H. Kim, T. W. Noh, E. J. Choi, and J. Yu, *Phys. Rev. B* **57**, R11043 (1998).
- ³⁶M. Quijada *et al.*, *Phys. Rev. B* **58**, 16093 (1998).
- ³⁷Ch. Hartinger, F. Mayr, J. Deisenhofer, A. Loidl, and T. Kopp, *Phys. Rev. B* **69**, 100403 (2004).
- ³⁸H. L. Liu, M. X. Kuo, J. L. Her, K. S. Lu, S. M. Weng, L. M. Wang, S. L. Cheng, and J. G. Lin, *J. Appl. Phys.* **97**, 113528 (2005).
- ³⁹When the sample is cooled from 300 K, $\text{Re}[\tilde{\epsilon}_{xx}]$ becomes negative at low frequencies.
- ⁴⁰R. Rauer *et al.*, *Appl. Phys. Lett.* **81**, 3777 (2002).
- ⁴¹C. Kooy and U. Enz, *Philips Res. Rep.* **15**, R388 (1960).
- ⁴²J. A. Cape and G. W. Lehman, *J. Appl. Phys.* **42**, 5732 (1971).
- ⁴³M. Hehn, S. Padovani, K. Ounadjela, and J. P. Bucher, *Phys. Rev. B* **54**, 3428 (1996).
- ⁴⁴V. Gehanno, A. Marty, B. Gilles, and Y. Samson, *Phys. Rev. B* **55**, 12552 (1997).
- ⁴⁵R. Bodenberger and A. Hubert, *Phys. Status Solidi A* **44**, K7 (1977).
- ⁴⁶A. Hubert and R. Schäfer, *Magnetic Domains* (Springer, Berlin, 1998).
- ⁴⁷J. Zak, E. R. Moog, C. Liu, and S. D. Bader, *J. Magn. Magn. Mater.* **89**, 107 (1990).
- ⁴⁸L. Uba, S. Uba, V. N. Antonov, A. N. Yaresko, T. Ślezak, and J. Korecki, *Phys. Rev. B* **62**, 13731 (2000).
- ⁴⁹M. S. Laad, L. Craco, and E. Müller-Hartmann, *New J. Phys.* **6**, 157 (2004).
- ⁵⁰G. Kresse and D. Joubert, *Phys. Rev. B* **59**, 1758 (1999).
- ⁵¹G. Kresse and J. Furthmüller, *Phys. Rev. B* **54**, 11169 (1996).
- ⁵²A. I. Liechtenstein, V. I. Anisimov, and J. Zaanen, *Phys. Rev. B* **52**, R5467 (1995).
- ⁵³S. W. Han *et al.*, *Phys. Rev. B* **69**, 104406 (2004).